Computational Modeling of Synthetic Jets

David C. Durán[*,1], Omar D. López[2]
[1]Mechanical Engineering Department, Universidad de los Andes, Bogotá - Colombia
*Corresponding author: Carrera 1ra No. 18A-12, da-duran@uniandes.edu.co

Abstract: A synthetic Jet actuator is a device which moves a fluid in and outside a cavity, through a small aperture, by the continuous oscillation of a diaphragm. This diaphragm is usually a piezoelectric disk which is excited by a sinusoidal voltage. The first approach to the problem was to validate the behavior of the piezoelectric disk through a tridimensional model, showing satisfactory results. After this validation an axisymmetric model of the complete (fluid + piezoelectric) synthetic jet actuator was implemented. This model was used to analyze the influence of the relevant dimensionless numbers in the synthetic jet formation when the disk was excited at low frequencies. Numerical results of this model show a strong dependence of the synthetic jet formation on the size of the aperture. Another relevant observation is that, for the case of synthetic jet formation, there is an interaction between the entering momentum and the diaphragm, which has not been observed in other synthetic jet models based only on Navier-Stokes solver. All these observations are of great help in synthetic jet device research and development, and encourage further multiphysics simulations and analysis of these actuators to be made.

Keywords: Synthetic Jet, Synjet, Structure-Fluid Interaction, Piezoelectric, Vortices

1. Introduction

A Synthetic Jet is defined as the time-averaged formation of escaping vortex rings from a cavity through which a fluid is suctioned and expelled, having a zero mass net flux but adding momentum to the surroundings. The device which generates Synthetic Jets is called a Synthetic Jet Actuator (SJA). A SJA is composed of three parts: The oscillating diaphragm, the resonant cavity and the orifice aperture as shown in Figure 1. SJA are widely used in a variety of engineering applications such as separation control, mixing, heat transfer and flow control in aerodynamics applications in which the use of these actuators can make separation more controllable, reducing drag, gaining lift, no buffet, less vibrations and noise (London Imperial College)

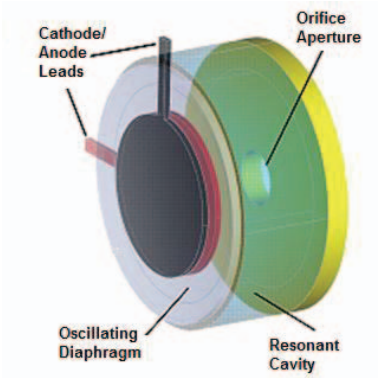

Figure 1. Tridimensional Schematic of the Synthetic Jet Actuator. (Morpheus Laboratory, University of Maryland, 2009)

Synthetic Jets are also attractive because they involve no net mass injection, they are lightweight and small in size; they also offer the possibility of not changing the original design of the wing or fuselage. In the area of airfoil flow control Synthetic Jet Actuators have the potential to replace the moving parts in wings which control the wing dynamics such as flaps, slats, ailerons, elevators and rudders. Synthetic Jets can also enhance heat transfer, by increasing small scale mixing near the heated surface, due to the vortex-dominated flow. The pulsating nature of Synthetic Jets enhances the mixing between the boundary layer and the mean flow and the entrained flow move the heated fluid out of the system according to Nuventix®[1]. These cooling devices can be used for LED, electronic parts heat dissipation or any other similar application. It can be seen that SJA have multiple applications, some of which can be truly revolutionary. This is the reason why the research on this topic is so important. SJA can be constructed and tested but this experimental approach is too expensive due to the high costs of the parts involved in constructing the actuators as well as the ones of the measuring methods. So, the best alternative for research on SJA is computer modeling. This has been done, until today, solving only the Navier-Stokes equations and including a known (from experimental data) boundary condition of velocity. However this is not the most

[1] http://www.nuventix.com

realistic approach to the problem since it ignores the multiphysics nature of the actuator. Willing to take into account the multiphysics nature of the problem and trying to make simulations more realistic, we modeled a SJA in COMSOL Multiphysics and studied the influence of different parameters in the SJ formation.

2. Use of COMSOL Multiphysics

2.1 Structure-Fluid Interaction Problem

The multiphysics interaction between the piezoelectric disk, which deforms due to the alternating voltage and the fluid, makes COMSOL Multiphysics the most suitable tool for the computational analysis of these devices. For this analysis, the Piezo Axial Symmetry, Incompressible Navier-Stokes and Moving Mesh ALE modules were used.

2.2 Piezoelectric Governing Equations

In a piezoelectric material an applied electric field E tends to align the internal dipoles, inducing stresses in the material equivalent to –eE by the, so called, inverse piezoelectric effect.

The coupled equations that model the inverse piezoelectric effects on the disk are:

$$\sigma = c^E \epsilon - e^T E \quad (1)$$

$$\rho \frac{\partial^2 u}{\partial t^2} = F \quad (2)$$

$$F = \nabla \cdot \sigma \quad (3)$$

$$\epsilon_{ij} = \frac{1}{2}\left(\frac{\partial u_j}{\partial x_i} + \frac{\partial u_i}{\partial x_j}\right) \quad (4)$$

Equation (1) is the constitutive equation for the piezoelectric material. In this equation the piezoelectric constant e relates the stress to the electric field in the absence of mechanical strain and c^E refers to the stiffness when the electric field is constant. Equations (2) to (4) are the classical elasticity equations which result in a good approximation to the piezoelectric disk deformation because it is expected to be little (in the order of mils. See figure 9). The piezoelectric material used in the diaphragm is called PZT-5A and its matrix properties are shown in tables 1 and 2.

Table 1. PZT-5A Elastic Constants (c^E, All entries x10^{10})

12.03	7.51	7.51	0	0	0
7.51	12.03	7.51	0	0	0
7.51	7.51	11.08	0	0	0
0	0	0	2.11	0	0
0	0	0	0	2.11	0
0	0	0	0	0	2.26

Table 2. PZT-5A dielectric constants (e)

0	0	0	0	12.2947	0
0	0	0	12.2947	0	0
-5.3512	-5.3512	15.7835	0	0	0

The disk is not only composed of the piezoelectric but also of a variety of other materials such as Copper and Stainless Steel which are bonded with a Si Adhesive. For this reason, the simulation included a metallic part in the subdomain. The disk is manufactured by FACE International (Face International Corporation, 2007).

2.3 Fluid Dynamics Governing Equations

The fluid can be described by the Incompressible Navier-Stokes equations:

$$\rho \frac{\partial \boldsymbol{u}}{\partial t} - \nabla \cdot [\mu(\nabla \boldsymbol{u} + (\nabla \boldsymbol{u})^T)] + \rho(\boldsymbol{u} \cdot \nabla)\boldsymbol{u} + \nabla \mathrm{p} = \mathbf{F} \quad (5)$$

$$\nabla \cdot \boldsymbol{u} = 0 \quad (6)$$

Equation (5) is the momentum transport equation and equation (6) is the equation of continuity. The variables in these equations are:

μ is the dynamic viscosity
ρ is the density
u is the velocity field
p is the pressure field
F is a volume force field (as gravity for example)

It was assumed that acoustic effects are negligible since any characteristic length (D or L) are larger than any acoustic wavelength. The Reynolds number in all simulations is laminar so no turbulence model is needed, as shown later in the results table.

2.4 Application Modules

- Piezo axial symmetry: This model solves the stress-strain equations for a piezoelectric material due to an applied voltage

- Incompressible Navier Stokes: This model solves the fluid motion according to Navier-Stokes equations
- Moving Mesh – ALE: This module is necessary to include a mesh that moves (solved by the piezo module) so that the fluid has the correct boundary conditions due to the deformation of the piezoelectric diaphragm

3. Theory on Synthetic Jets Formation

According to (Holman, Utturkar, Mittal, Smith, & Cattafesta, 2005) a synthetic jet is formed when the inverse of the Strouhal number is larger than a constant i.e:

$$If\ \frac{1}{Sr} > C\ \rightarrow jet \quad (7)$$

Where Sr is the Strouhal Number and constant C depends on the geometry of the problem. Holman et al obtained a value of C in the order of one, using an actuator of 5.50 x $10^{-6}m^3$ of volume, an orifice diameter of 2.00 mm and an orifice thickness of 1.65 mm and edges with a curvature of 0.15 (Holman, Utturkar, Mittal, Smith, & Cattafesta, 2005). The inverse of the Strouhal number is the ratio between the Reynolds number and the square of the Stokes number

$$\frac{1}{Sr} = \frac{Re}{S^2} \quad (8)$$

The Reynolds number is shown in equation (9):

$$Re = \frac{\rho U d}{\mu} \quad (9)$$

Where U is a characteristic velocity of the flow (in the present work U is defined as the maximum instantaneous velocity i.e. U = max(u)), d is the diameter of the aperture. The Stokes Number is given by

$$S = \sqrt{\frac{\omega d^2}{\upsilon}} \quad (10)$$

Where ω is the oscillation frequency in rad/s, d is the diameter of the aperture and υ is the kinematic viscosity of the fluid

4. Models

4.1 3-D Piezoelectric Disk Modeling

The first approach to the problem was to develop a 3-D piezoelectric model of the diaphragm (Figure 2). This model was tested at different voltages to observe the deformation corresponding to each one of them and to validate the piezoelectric model of the disk.

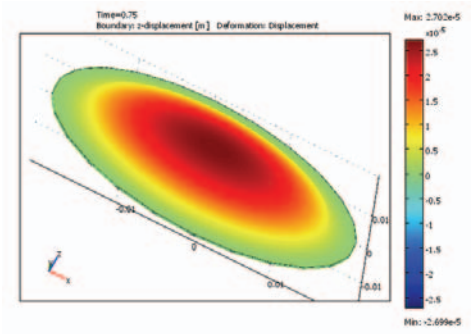

Figure 2. 3-D Model of the diaphragm

4.2 Axisymmetric Synthetic Jet Actuator Model

The results of the 3D model showed that the most relevant deformations occur in the z and radial directions. For these reasons and due to the computational resources available, an axisymmetric model was implemented.

4.2.1 Axisymmetric Disk Modeling

4.2.1.1 Subdomain Settings

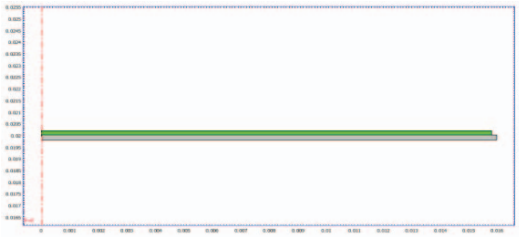

Figure 3. Geometry of the piezoelectric diaphragm.

In Figure 3 the green area shows the piezoelectric material portion of the diaphragm while the gray area shows the metallic component of the diaphragm.

4.2.1.2 Boundary Settings

Figure 4 shows the boundaries used in the piezoelectric module, these are described in Table 3. It is also assumed that there is no relative displacement between the piezoelectric and the metallic portions of the diaphragm. Boundaries 2, 3, 4 and 7 are set free since these are the ones that move when the disk is excited. Boundary 1 emulates the fixed side of the disk.

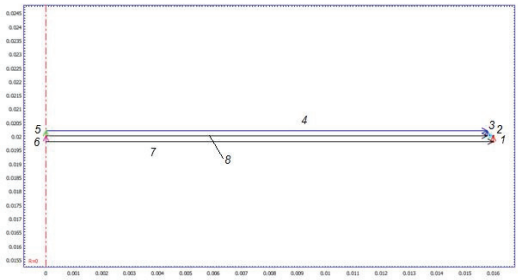

Figure 4. Numbering of the boundaries

Table 3. Piezoelectric Disk Boundary Conditions

Boundary	Structural	Electrical
1	Fixed	Continuity
2	Free	Continuity
3	Free	Continuity
4	Free	V0*sin(ωt)
5	Axial Symmetry	Continuity
6	Axial Symmetry	Continuity
7	Free	Continuity
8	-	Ground

Where: V is the instant electric potential, V_0 is the electric potential's amplitude. The diaphragm is designed for Electric Potentials between 0 and 500 V, so the values chosen for V_0 are in this range. Since this is a low frequency study ω was fixed at 2π rad/s.

4.3 Axisymmetric Fluid Dynamics Model and Boundary Conditions

4.3.1 Subdomain Settings

The fluid subdomain includes all the fluid contained inside and outside the cavity. Though this is one subdomain, one can clearly distinguish between the fluid that is inside the cavity and the fluid outside.

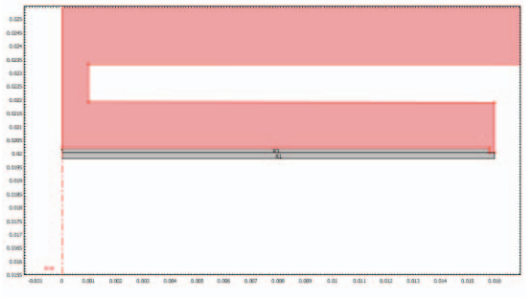

Figure 5. Fluid subdomain close-up.

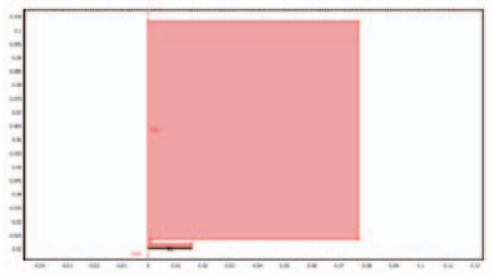

Figure 6. Whole Fluid subdomain.

In Figures 5 and 6 the red area is the fluid subdomain. In Figure 6, the subdomain in the outside must be large enough so that the boundary conditions do not affect the Synthetic Jet, for this reason the horizontal edge of the outside domain is three times larger than the radius of the diaphragm while the vertical edge is five times this size.

4.3.2 Boundary Settings

Figures 7 and 8 show all the boundaries involved in the fluid model. Interior boundaries are not taken into account and all the boundaries of the disk are considered moving walls, which movement is determined by the deformation of the piezoelectric disk. Boundaries 13 and 14 are considered open.

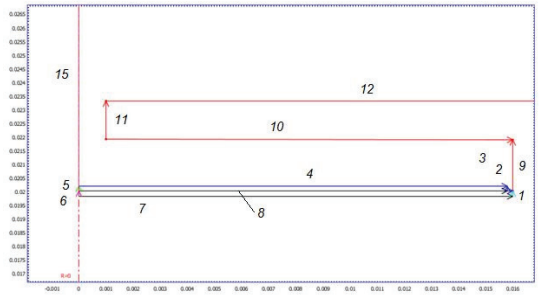

Figure 7. Fluid Boundaries Close-Up

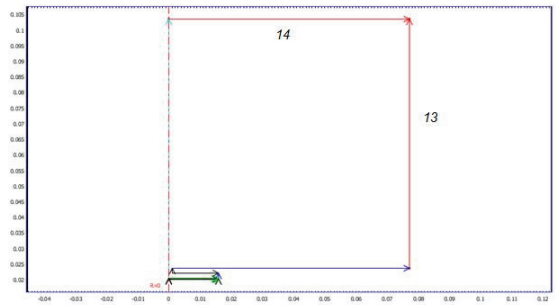

Figure 8. Fluid Boundaries

Table 4. Fluid Boundaries

Boundary	Fluid	Boundary	Fluid
1	-	9	Wall
2	Moving Wall	10	Wall
3	Moving Wall	11	Wall
4	Moving Wall	12	Wall
5	Symmetry	13	Open
6	Symmetry	14	Open
7	-	15	Symmetry
8	-		

5. Numerical Results

5.1 3-D Piezoelectric Disk Modeling

The results of the 3D piezoelectric disk model are shown in Figure 9, in which the red triangles show the results of the numerical simulations, while the black dots and curve show the performance given by the manufacturer. It is observed that the experimental results tend to be linear while the black curve tends to be linear only under 300 V p-p. For this reason most of the experiments are performed in the range 0-300V p-p. The percentages in Figure 9 show the difference between the numerical simulations and the manufacturer experimental results. Between 0-300V the error is about 9% on average.

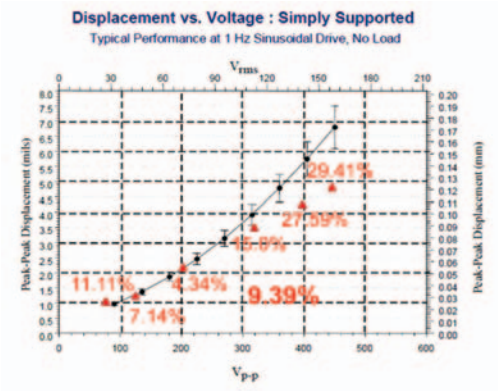

Figure 9. Displacement vs Voltage. (Face International Corporation, 2007)

5.2 Low 1/Sr

Figure 10 shows the moment when the vortex ring starts forming in the outside due to the outwards movement of the fluid inside the cavity.

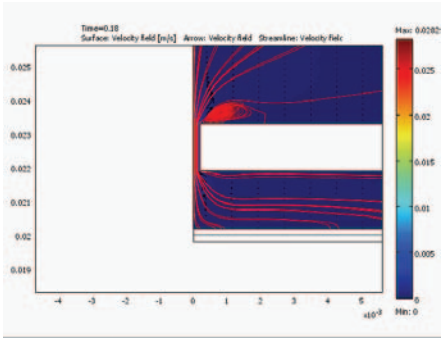

Figure 10. Low 1/Sr at time 0.18.

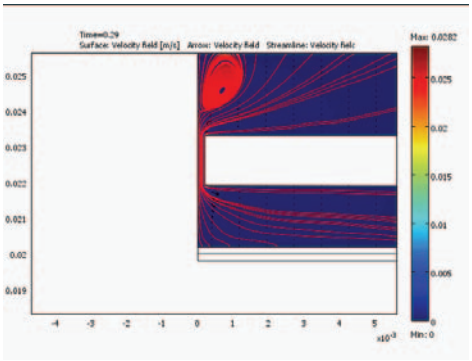

Figure 11. Low 1/Sr at Time 0.29.

The vortex ring tries to escape from the aperture but instead it is swallowed again through the aperture as shown in Figure 11

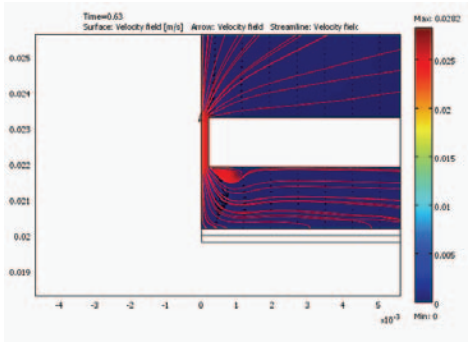

Figure 12. Low 1/Sr at Time 0.73.

Figure 12 shows the swallowed vortex ring appearing inside the cavity as the fluid moves inwards.

5.3 High 1/Sr

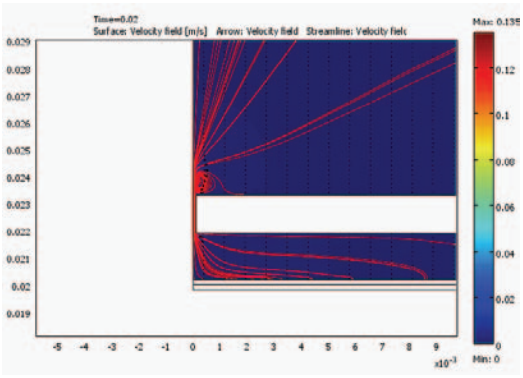

Figure 13. High 1/Sr at Time 0.02

Figure 13 shows how; as the fluid flows outwards, a tiny vortex ring appears outside the cavity.

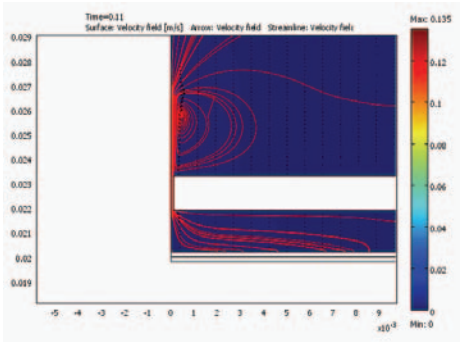

Figure 14. High 1/Sr at Time 0.11.

Figure 14 shows how the vortex ring escapes away from the aperture, so that it cannot be swallowed inside the cavity again and evolves as shown below (Figure 15)

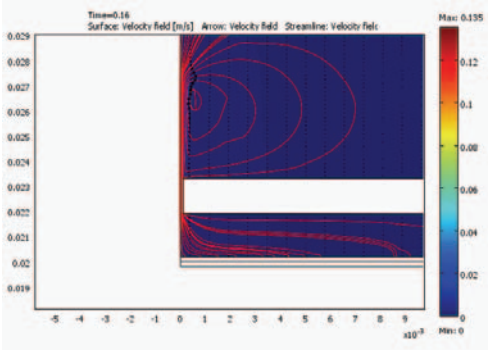

Figure 15. High 1/Sr at Time 0.16.

6. Discussion

Table 5 (Appendix 1) describes the results obtained in different experiments, for which different parameters where changed. Experiments 1-3 show no significant change in the inverse of the Strouhal Number when varying the electric potential in one order of magnitude. For these experiments no jet formation is observed. For experiment 4 and 5 a change of one order of magnitude was applied to the aperture's diameter, afterwards two experiments in which the electric potential was varied were done, obtaining a significant increase in the inverse of the Strouhal Number, although no jet formation was observed. For this reason the diameter of the aperture will be held in the order of 10^{-4} and other parameters changed. In experiments 8 to 11 the previous aperture's size was maintained and the viscosity was varied, obtaining inverse Strouhal numbers greater than 100 and observing jet formation.

7. Conclusions

- **The fluid velocity is weakly dependant of the applied voltage.** Keeping in mind that the applied voltage must be only in a certain range (under 300 V), the model was proved for several voltages. When arriving near 300 V no significant increase was observed in the inverse of the Strouhal number. For this reason the voltage was increased even outside of the range (until 500 V) but no significant change was observed.
- **The fluid velocity is strongly dependant of the aperture diaphragm.** When varying the aperture diaphragm dimension in one order of magnitude, the inverse of the Strouhal number varies almost in two orders of magnitude. This is due to the mass conservation because through a smaller diameter the fluid will flow at a higher speed increasing the Reynolds Number and, thus, the Strouhal Number.
- **The jet formation criterion for this problem is in the order of hundreds.** After running several simulations of the model, it is seen that when the inverse of the Strouhal number is near one hundred a clear vortex formation and escape is differenced. An exact number can't be given for this criterion since there exists always a transition zone between the jet and no jet formation.
- **There exists vortex ring formation in the inside of the cavity.** Never before, with the

classical one-physics simulations, an interaction of the vortex formation inside the cavity and the diaphragm has been observed. This is due to the diaphragm deformation and its wall condition, which makes the entering vortex to hit the diaphragm and start an interaction with it.

8. Future Work

- Coupling of the acoustics module to the model
- Comparison with Lumped Element Modeling results
- Study the influence of the vortex rings interactions with the diaphragm in the quality of SJ formation
- Study of the influence of the actuator's height
- Study of the influence of the frequency in the SJ formation
- Study of the phenomena according to a turbulence model

9. References

1. Alan Barnett et al, Finite Element Approach to Model and Analyze Piezoelectric Actuators, *JSME International Journal*, 476-485 (2001)
2. Quentin Gallas et al, Lumped Element Modeling of Piezoelectric-Driven Synthetic Jet Actuators, *AIAA Journal*, 240-247 (2003)
3. Ryan Holman, Formation Criterion for Synthetic Jets, *AIAA Journal*, (2005)
4. Uno Ingard, On the Theory and Design of Acoustic Resonators, *The Journal of the Acoustical Society of America*, 1037-1061 (1953)
5. Poorna Mane et al, Experimental design and analysis for piezoelectric circular actuators in flow control applications, *Smart Materials and Structures* (2008)
7. Vincent Piefort, Finite Element *Modelling of Piezoelectric Active Structures*, Ph.D. thesis. Bruxelles, Belgium: Université Libre de Bruxelles, Department for Mechanical Engineering and Robotics (2001)
8. Christopher Rumsey, *Proceedings of the 2004 Workshop on CFD Validation of Synthetic Jets and Turbulent Separation Control*, Hampton, Virginia: NASA. (2007)
9. B. Smith et al, The Formation and Evolution of Synthetic Jets, *Physics of Fluids*, 2281-2297 (1998)
10. Yukata Takagi et al, Dielectric Properties of Lead Zirconate, *Journal of the Physical Society*, 208-209 (1951)
11. David Durán et al, *Computational Modeling of Synthetic Jets*, Mechanical Engineering Thesis (2010)

10. Acknowledgements

The authors would like to thank the Departments of Mechanical and Chemical Engineering of the Universidad de los Andes which financially supported this project.

11. Appendix

Table 5. Simulations Results Summary

Exp. No.	Diam. (m)	height (m)	Potential (V)	viscosity (Pa.s)	Vel max. (m/s)	Reynolds	Stokes	1/Sr	Criterion
1	2e-03	1.4e-03	25	1e-06	3.27e-03	6.54	5.01	**0.26**	**no jet**
2	2e-03	1.4e-03	50	1e-06	3.27e-03	6.54	5.01	**0.26**	**no jet**
3	2e-03	1.4e-03	200	1e-06	3.02e-03	6.05	5.01	**0.24**	**no jet**
4	2e-04	1.4e-03	100	1e-06	1.21e-01	24.2	0.50	**96.29**	**no jet**
5	2e-04	1.4e-03	500	1e-06	1.21e-01	24.2	0.50	**96.29**	**no jet**
6	2e-04	1.4e-03	100	1e-07	0.135	270	1.59	**107.43**	**jet**
7	2e-04	1.4e-03	100	1e-06	0.146	29.2	0.50	**116.18**	**jet**